Published in final edited form as:
Semin Oncol. 2011 February ; 38(1): 26–41. doi:10.1053/j.seminoncol.2010.11.001.

Metabolic Tumor Imaging Using Magnetic Resonance Spectroscopy

Kristine Glunde[a,b] and **Zaver M. Bhujwalla**[a,b]

[a] Russell H. Morgan Department of Radiology and Radiological Science, Johns Hopkins University School of Medicine, Baltimore, MD

[b] Sidney Kimmel Comprehensive Cancer Center, Johns Hopkins University School of Medicine, Baltimore, MD

Abstract

The adaptability and the genomic plasticity of cancer cells, and the interaction between the tumor microenvironment and co-opted stromal cells, coupled with the ability of cancer cells to colonize distant organs, contribute to the frequent intractability of cancer. It is becoming increasingly evident that personalized molecular targeting is necessary for the successful treatment of this multifaceted and complex disease. Noninvasive imaging modalities such as magnetic resonance (MR), positron emission tomography (PET), and single-photon emission computed tomography (SPECT) are filling several important niches in this era of targeted molecular medicine, in applications that span from bench to bedside. In this review we focus on noninvasive magnetic resonance spectroscopy (MRS) and spectroscopic imaging (MRSI) and their roles in future personalized medicine in cancer. Diagnosis, the identification of the most effective treatment, monitoring treatment delivery, and response to treatment are some of the broad areas into which MRS techniques can be integrated to improve treatment outcomes. The development of novel probes for molecular imaging—in combination with a slew of functional imaging capabilities—makes MRS techniques, especially in combination with other imaging modalities, valuable in cancer drug discovery and basic cancer research.

Despite a reduction in the overall mortality from cancer, one in four deaths in the United States alone is still attributable to this disease.[1] Functional imaging promises to play an important role in the management of cancer patients.

Magnetic resonance spectroscopy (MRS) techniques are based on the principle that it is possible to detect radiofrequency (RF) signals generated by magnetic nuclear spins of magnetic resonance (MR) active nuclei such as ^{1}H, ^{31}P, ^{13}C, and ^{19}F precessing in an external magnetic field B_0. This detection is only possible after excitation with an RF pulse transmitted by an RF coil at the magnetic resonance frequency ω_0. The magnetic resonance frequency ω_0 is linearly dependent on B_0 and on the gyromagnetic ratio of the nucleus γ, as $\omega_0 = \gamma B_0$. The MR signal intensity depends on the concentration and the gyromagnetic ratio of the nuclear spins and two rate constants that govern the time dependence of the magnetization signal: the spin-lattice or longitudinal relaxation time, T_1, and the spin-spin or transverse relaxation time, T_2. After acquisition of the free induction decay (FID) of these

Address correspondence to Kristine Glunde, PhD, Department of Radiology, Johns Hopkins University School of Medicine, 212 Traylor Bldg, 720 Rutland Ave, Baltimore, MD 21205. kglunde@mri.jhu.edu.

Financial disclosures: The authors have nothing to disclose.

RF signals, the FID is Fourier-transformed, and phase and baseline corrections are performed to obtain an interpretable MR spectrum.

MRS provides information about the chemical environment of the nuclear spin such as number of chemical bonds, neighboring nuclei, and overall chemical structure. The presence of an electron cloud surrounding a particular nucleus creates an electronic shield that lowers the B_0 magnetic field to which this nucleus would normally be exposed. This resonance frequency difference, which is also referred to as chemical shift, is expressed as parts per million or ppm, a value that is independent of the magnetic field strength. Chemical shift values in ppm thus provide information about the molecular group carrying a particular nucleus, and correspond to a change in the resonance frequency of this nucleus within the molecules, as a function of their chemical bonds. Chemical shifts are frequently reported relative to a reference resonance frequency, such as, for example, tetramethylsilane.

MR spectra can be acquired with or without spatial localization. In the absence of localization, the signal is acquired from the entire sensitive region of the coil that detects the RF signal. Localized spectra can either be acquired from a single volume element (single-voxel), or from multiple voxels (multi-voxel). In chemical shift imaging (CSI), phase-encoding gradients are incorporated to generate images of signals obtained at different chemical shifts by spatially encoding chemical shift information. Phase-encoding can be applied in one, two, or three spatial dimensions. CSI is especially useful in heterogeneous tissues such as tumors. Localized spectra can be processed to obtain images from individual metabolites.

Some of the applications of MRS in cancer are summarized in Table 1 and demonstrate the breadth of this modality in characterizing tumor metabolism, pH, hypoxia, drug delivery, treatment efficacy, and apoptosis. With its ability to identify different compounds by their chemical shifts, MRS is especially useful in studying metabolism. Due to aberrations in their genome and proteome, cancer cells exhibit a unique metabolic phenotype characterized by high glucose uptake, increased glycolytic activity and lactate production, decreased mitochondrial activity, low bioenergetic status, and aberrant phospholipid metabolism.[2–4] Additionally, tissue-specific metabolites such as N-acetyl-aspartate (NAA) in the brain, and citrate in the prostate, display an MRS-detectable decrease as the cancer cell population in the tissue expands, thereby reducing the number of normal cells.[4–6] Proton or ^{31}P MRS or MRSI detection of these endogenous metabolites has proven useful in the diagnosis of cancer,[7–14] and in monitoring anticancer therapy in some instances, as detailed in subsequent sections. Importantly, MRS characterization of the aberrant cancer cell metabolism has led to the identification of related enzymes as novel anticancer targets.[3,15–18] MR biomarkers, such as the total choline (tCho) signal, are already being explored in the clinical setting for characterizing tumors and the response of tumors to anticancer therapy.[19–21] Elevated metabolites in choline phospholipid metabolism present unique targets to exploit for molecular targeting, the outcome of which can be noninvasively detected and imaged by MRSI.[15,22] Several pharmacological and molecular approaches are already being developed to target choline metabolism, and specifically choline kinase (Chk) activity, as discussed in detail below.

Advances in pulse sequence design for MRS/I, development of novel substrates, probes, and drugs, and technological advances have further advanced and diversified the use of MRS/I in cancer discovery and treatment. Here we have reviewed some recent biomedical applications of ^{1}H, ^{13}C, ^{31}P, and ^{19}F MRS in preclinical models of cancer and have summarized new developments, such as the hyperpolarization of ^{13}C spins to increase the MR detection sensitivity of ^{13}C-labeled substrates.

^{1}H AND ^{31}P MRS OF CHOLINE PHOSPHOLIPID METABOLISM

Choline phospholipid metabolism is profoundly altered in cancer cells.[3,23–25] Almost every tumor type investigated has revealed elevated phosphocholine (PC) and increased tCho-containing metabolites.[3,23–25] Malignant transformation has been found to alter the profile of the choline compounds glycerophosphocholine (GPC) and PC in breast[26] and ovarian[27] cancer cells. In high-resolution ^{1}H and ^{31}P MR spectra of breast[26] and ovarian[27] cell extracts, GPC was higher than PC in normal cells but switched to being lower than PC in cancer cells. Proton or ^{31}P MRS can detect these endogenous metabolic changes in vivo, and in tumor tissue biopsies or cancer cells ex vivo, as shown for MDA-MB-231 human breast cancer cells and tumor xenograft models in Figure 1. Proton MRS signals from water-soluble choline metabolites arise between 3.2 and 3.3 ppm from the nine chemically equivalent protons in the choline $–N(CH_3)_3$ groups, which are displayed as color-coded ^{1}H nuclei corresponding to MR signals with the same color-code in the representative spectra in Figure 1. Because nine protons contribute to this signal, it displays a higher signal intensity than the ^{1}H signals in the methylene groups of the same choline metabolites, which only contain two equivalent protons each (see Figure 1). Using 3-(trimethylsilyl)propionic-2,2,3,3-d_4 acid as a chemical shift reference at pH 7.4, free choline (Cho) is detected at 3.21 ppm, PC at 3.23 ppm, and GPC at 3.24 ppm, in high-resolution ^{1}H MR spectra of cell or tissue extracts (see Figure 1), or in high-resolution magic angle spinning (HR MAS) ^{1}H MR spectra of biopsies (see Figure 2). The chemical structures of Cho, PC, and GPC are shown in Figure 1. It is not possible to resolve Cho, PC, and GPC in vivo, even at higher magnetic field strengths, because of the broader line widths that result from magnetic field inhomogeneities. Instead, a single tCho peak comprised of these three signals is detected, as shown in Figure 1. Clinical multicenter trials are currently underway to establish single-voxel ^{1}H MRS, covering a breast lesion for breast cancer detection. Multi-voxel in vivo ^{1}H MRSI of one or multiple slice(s) through a region of interest provides multiple spectra from a slice or volume of tissue, which can be processed to obtain the spatial distribution of tCho or other metabolites.

Phosphorus-containing choline metabolites can also be detected with ^{31}P MRS, as demonstrated in Figure 1. Following chemical shift calibration to a reference compound such as methylene diphosphonic acid at 18 ppm, a signal from PC at 3.9 ppm and GPC at 0.5 ppm is observed in high-resolution ^{31}P MR spectra of cell or tumor extracts, as shown by color-coded signals and their corresponding ^{31}P nuclei with the same color-code in the chemical structures. In the in vivo setting, a mixed phosphomonoester (PME) signal containing unresolved PC and phosphoethanolamine (PE) resonances, and a mixed phosphodiester (PDE) signal containing unresolved GPC and glycerophosphoethanolamine (GPE) resonances are observed in ^{31}P MR spectra (see color-coding in Figure 1). Since in routine in vivo settings neither ^{1}H nor ^{31}P MRS are able to spectrally resolve Cho, GPC, and PC as individual signals, changes in PME, PDE, and tCho detected in vivo in ^{31}P and ^{1}H MR spectra often stem from concentration changes of a number of metabolites. Acquiring consecutive proton-decoupled ^{31}P and ^{1}H MR spectra can, in some cases, overcome this problem.[28] A recent clinical study demonstrated the feasibility of partially resolving PC from PE, and GPE from GPC by using ^{1}H-decoupled ^{31}P MRS at 1.5 T[29] and at the higher field strength of 3T that is also clinically available. In clinical studies ^{1}H MRS is preferred over ^{31}P MRS because of its higher sensitivity and standard availability on clinical scanners. A recent study reported a novel ^{1}H to ^{31}P polarization transfer method on a clinical 3T MR scanner that resulted in a more than twofold increase of signal-to-noise ratio compared to direct ^{31}P MRS methods.[30] Proton to ^{31}P polarization transfer in this study was achieved by applying chemical shift selective refocusing pulses at 3T.[30] These pulses canceled the homonuclear J-coupling effects that attenuated ^{31}P signals from PE, PC, GPE, and GPC.[30]

Identification of PE, PC, GPE, and GPC in human brains was possible with this method, providing a voxel size of 2 × 2 × 2 cm^3 in a three-dimensional MRSI data set.[30]

The molecular causes for the increased PC and tCho levels in cancer cells and tumors are an increased expression and activity of Chk,[17] a higher rate of choline transport,[31,32] and an increased phospholipase C and D activity.[27,33] These enzymes, among others, constitute the biosynthetic and breakdown pathways of the major membrane phospholipid phosphatidylcholine (PtdCho).[22] GPC, PC, and Cho are precursors and breakdown products of PtdCho.[22] Chk[3,15–18] and PtdCho-specific phospholipase D[34] and C[27] have recently been targeted by gene silencing or enzyme inhibition in studies of MRS-monitored, targeted anticancer therapies, as discussed in detail below. Growth factor signaling, cytokine action, oncogene activation, and chemical carcinogenesis impact on the enzymes in choline phospholipid metabolism.[3,23,24]

^{1}H MRS OF MOBILE LIPIDS

In addition to choline metabolites, in vivo single-voxel ^{1}H MRS and multi-voxel MRSI detect signals from lipid metabolism-related compounds, such as the methylene signal at 1.3 ppm, and the methyl signal at 0.9 ppm (see representative ^{1}H MR spectra in Figure 1). These methylene and methyl signals originate from CH_2 and CH_3 groups, respectively, in fatty acyl chains of triacylglycerides that form mobile lipid droplets in the cytoplasm of intact cancer cells or in the intercellular space of solid tumors.[35,36] Membrane lipids do not contribute to these lipid signals at 1.3 and 0.9 ppm because the low mobility of membrane lipids limits their detection by MRS in vivo.[35,36] The CH_2 lipid signal at 1.3 ppm overlaps with the lactate signal at 1.3 ppm, and requires spectral editing for the separation of these two signals.[37–39] Additionally, mobile polyunsaturated fatty acyl chain signals can be detected at 5.4 and 2.8 ppm, and can be used to assess polyunsaturation of mobile lipids.[36] However, the signal at 5.4 ppm may be difficult to detect because of its proximity to the large water signal at 4.7 ppm.[36] Significantly higher levels of lipid have been detected in high-grade human gliomas compared to low-grade gliomas, suggesting a potential application of the lipid signal at 1.3 ppm in tumor grading.[35] Intratumoral lipid droplets also have been shown to correlate with drug resistance or response.[35] Cytoplasmic accumulation of triacylglycerides in cancer cells and tumors has been attributed to diverse biological processes such as hypoxia, degeneration of mitochondria, differentiation, growth arrest, and apoptotic cell death.[35,36,40] Increased diacylglycerol and triacylglycerol biosynthesis in lipid metabolism can lead to the formation of triacyglycerides.[36,40] The mobile lipid signal also has been observed to change with apoptosis, necrosis, or lipid droplet formation.[41–43]

^{31}P MRS OF ENERGY METABOLISM AND PH

Because ^{31}P MRS detects signals from energy metabolites and breakdown products such as nucleoside triphosphates (NTPs), nucleoside diphosphates (NDPs), phosphocreatine (PCr), and inorganic phosphate (Pi) (see Figure 1), it is ideally suited to investigate tumor energy metabolism in vivo. Importantly, tumor pH can be determined from the chemical shift of the Pi resonance as described below. However, its use has declined in recent years, especially for clinical studies, because of poor sensitivity. The bioenergetic state of cancer cells is relatively low because of the Warburg effect.[44] The production of high-energy phosphates such as NTP and PCr depends on available glucose and oxygen, which are delivered to tumors through blood vessels. Therefore, energy metabolism is tightly coupled to tumor blood flow,[45,46] and decreases in hypoxic regions. ^{31}P MRS may be useful in detecting changes in tumor reoxygenation during radiation therapy that are mediated by changes in blood flow, as indicated in preclinical studies.[47,48]

The initial observation by Moon and Richards[49] that the chemical shift of intracellular phosphates in whole blood is sensitive to pH led to the development of using the chemical shift of the Pi peak to measure tissue pH with ^{31}P MRS. Although the Pi signal in tissues consists of both intra- and extracellular Pi, in tumors the Pi signal is primarily of intracellular origin,[50] and the chemical shift of Pi reports intracellular pH (pHi). Since tumors are highly glycolytic, it was assumed for many decades that tumor pH was acidic, and indeed these assumptions were supported by electrode measurements of tumor pH.[51] However, ^{31}P MRS measurements of tumor pH revealed that tumor pHi was typically neutral or alkaline.[52] The subsequent development of an extracellular pH (pHe) probe, 3-aminopropylphosphonate, 3-APP,[53,54] enabled simultaneous detection of intra- and extracellular pH in tumors, and confirmed that the pHe of tumors is acidic, while the pHi is neutral-to-alkaline. The acidic pH within the tumor microenvironment can significantly influence several phenotypic characteristics, and the ability to measure tumor pH noninvasively is therefore important in oncological research. Acidic pHe can stimulate cancer cell invasion in culture.[55] Chronic or acute treatment with bicarbonate can increase pH in vivo.[56] A recent study demonstrated that mice treated with bicarbonate developed significantly fewer metastases.[57] Intracellular pH has been measured in human cancers using ^{31}P MRS,[23] but probes to measure pHe in humans are not yet available. The low sensitivity of ^{31}P MRS does not allow acquisition of spectra with high spatial resolution. To date, ^{31}P MR spectra can be acquired from 3- to 4-mm thick tumor slices, or from large voxels of approximately $6 \times 6 \times 6$ mm^3 localized to the tumor.

To overcome the sensitivity limitations of ^{31}P MRS, ^{1}H and ^{19}F MRS probes also have been developed to measure pHe.[58–60] ^{1}H MRS probes are based on imidazole compounds and have been used to measure localized tumor pH using MRSI with spatial resolutions approaching $1 \times 1 \times 1$ mm^3.[54,59,61] One imidazole-based compound, 2-imidazole-1-yl-ethoxy carbonyl propionic acid (IEPA), has been used to image tumor pHe in tumor models. Consistent with earlier findings, the probe reported an acidic and heterogeneous pHe.[54,59]

High-Resolution Magic Angle Spinning MRS

HR MAS ^{1}H MRS is a relatively new technique for examining intact biological tissue ex vivo at high spectral resolution.[6,62–64] HR MAS ^{1}H MRS can be particularly useful in the clinic for analyzing the metabolome of biopsy specimens prior to pathological classification.[6,62–64] By spinning the solid sample at a frequency of typically 1 to 70 kHz at the magic angle of θ_m, which is circa 54.74° and where $\cos^2\theta_m$ equals 1/3, with respect to the direction of the magnetic field, the normally broad lines become narrower, increasing the resolution for better identification and analysis of the spectrum.[6,62–64] The major advantage of HR MAS ^{1}H MRS is that, in contrast to high-resolution MRS of tissue extracts, the tissue can be used for subsequent histologic, biochemical, and genetic analyses.[6,62–64] An example of HR MAS ^{1}H MRS of clinical breast cancer specimens shown in Figure 2 demonstrates the sensitivity of this technique.[65] A combination of principal component analyses and automated neural network applications is typically used to process the rich data sets obtained with HR MAS ^{1}H MRS (see Figure 2).[65] This approach was able to detect the metabolic phenotype of tumors, as evident from the derived score plot of three principal components shown in Figure 2, in which healthy adjacent breast tissue was clearly separated from cancer tissue, demonstrating a marked metabolic difference between healthy breast and breast tumor tissue.[65] HR MAS ^{1}H MRS may, in the future, be used to complement histopathological analysis for detecting and characterizing cancers.[65]

^{13}C MRS TECHNIQUES TO DETECT LABELED SUBSTRATES

^{13}C MRS is useful to detect ^{13}C-labeled metabolites following administration of suitable ^{13}C-labeled substrates in cancer cells and solid tumors. ^{13}C MRS has been applied

to study glycolysis, choline metabolism,[22] or other metabolic pathways. ^{13}C MRS is used to detect the incorporation of a ^{13}C label, which is introduced into the system as a ^{13}C-labeled substrate, within downstream metabolites and products. The flux of substrates through metabolic pathways can be derived by metabolic modeling. Unfortunately, direct detection of ^{13}C nuclei by ^{13}C MRS suffers from low sensitivity. The ^{13}C MRS sensitivity can be improved by magnetization transfer techniques, such as nuclear Overhauser effect (NOE) methods, heteronuclear cross-polarization experiments,[66] and indirect inverse detection methods.[67] These methods improve the detection sensitivity of ^{13}C nuclei making it comparable to that of ^{1}H MRS, for in vivo studies. To enhance ^{13}C signals, magnetization from neighboring protons is transferred through space using dipole-dipole spin coupling in NOE methods, or through chemical bonds using the J-coupling between ^{13}C and ^{1}H spins. The enhanced ^{13}C signals are detected directly with broadband proton decoupling in direct detection methods, such as NOE, distortionless enhancement by polarization transfer (DEPT), insensitive nuclei enhanced by polarization transfer (INEPT), and heteronuclear cross-polarization. In indirect detection schemes such as heteronuclear multiple quantum coherence (HMQC) and heteronuclear single quantum coherence (HSQC) methods, the magnetization is transferred from ^{1}H to ^{13}C and then back to ^{1}H. In HMQC and HSQC, the ^{13}C signals are indirectly detected as ^{1}H frequencies, achieving significantly enhanced sensitivity due to the higher gyromagnetic ratio γ of ^{1}H.[67]

^{13}C MRS OF ^{13}C-LABELED GLUCOSE/LACTATE

Since a high glycolytic activity is a common feature of many cancers, ^{13}C MRS of ^{13}C-labeled glucose has been used to study glycolysis in tumors. Cancer cells undergo glycolysis even in the presence of oxygen,[44,68] referred to as the “Warburg effect” after Otto Warburg who observed this phenomenon in 1930. Glycolysis is regulated by multiple oncogenes and signaling pathways.[44] Glycolysis in cancer cells occurs under well-oxygenated conditions, in part, through the stabilization of hypoxia-inducible factor alpha (HIF-1α).[68] Specifically, HIF-1α increases the formation of lactate dehydrogenase, which converts pyruvate to lactate; HIF-1α also activates pyruvate dehydrogenase, which converts pyruvate to acetyl-coenzyme A.[69] Additionally, poor blood flow and the resulting hypoxia also contribute to increased anaerobic glycolysis in tumors.[51,70] Increased expression of the glucose transporters GLUT-1 and -3, among others, in cancer cells also increases glucose uptake of tumors.[71] Overall, the combination of increased glucose uptake with increased glycolysis results in cancer cells rapidly metabolizing glucose to form lactate. The kinetics of [3-^{13}C]-labeled lactate formation can be determined by delivering [1-^{13}C]-labeled glucose through an intravenous infusion. Determining the kinetics of ^{13}C-labeled substrates over time facilitates the study of glucose uptake, delivery, and glycolytic breakdown, as well as lactate synthesis and clearance from the tumor.[72] Lactate levels in tumors are determined by several factors, such as tumor hemodynamics, substrate supply, hypoxia, venous clearance, glucose supply, extent of necrosis, and degree of inflammatory cell infiltrate.[73] For example, volume localized ^{13}C MRS with ^{1}H-^{13}C cross polarization was applied to detect the conversion of [1-^{13}C]-glucose to [3-^{13}C]-lactate in a murine mammary carcinoma model, and demonstrated that decreasing tumor oxygenation correlated with increasing glycolytic rate.[74] High-resolution ^{13}C MRS studies of tumor or organ extracts are useful in animals infused with [1-^{13}C]- or [U-^{13}C]-labeled glucose.[75] Such studies can reveal complex ^{13}C-labeling patterns in several metabolites, providing insight into metabolic compartmentalization, shuttling of metabolites between cell types or organs, and metabolic fluxes.[75]

HYPERPOLARIZED ^{13}C MRS

The use of hyperpolarized ^{13}C-labeled substrates has revitalized ^{13}C MRS studies because of the large increase in ^{13}C detection sensitivity achieved by hyperpolarization.[76,77]

Dynamic nuclear polarization (DNP) for solution-state MRS (DNP-MRS) can, in theory, increase the ^{13}C detection sensitivity of hyperpolarized ^{13}C-labeled substrates and their metabolites by up to 10,000-fold.[76,77] To achieve DNP, homogeneously distributed organic free radicals are added to the sample before cooling it, to fulfill the requirement for unpaired electrons.[78] Once cooled and in the solid state, the high electron spin polarization of the sample is transferred to the nuclear spins by microwave irradiation.[78] Subsequently, the sample is brought into a liquid solution after rapid dissolution.[78] This method makes it possible to bring polarized, cold, solid samples into solution while preserving their nuclear polarization for a short time, which is sufficient for ^{13}C MRSI,[78] as evident in Figure 3.[77] Complexities in achieving hyperpolarization in the solid state, the appropriate free radicals, and the limited number of molecules amenable reduce the actual, achievable increase in ^{13}C detection sensitivity of hyperpolarized ^{13}C-labeled substrates. DNP-MR spectrometers and hyperpolarizers are currently becoming commercially available. Elevated lactate and possibly alanine produced from hyperpolarized [1-^{13}C]-labeled pyruvate are under investigation as noninvasive biomarkers to determine the presence and histologic grade of cancers in preclinical models,[77] as shown in Figure 3. It may be possible to translate these preclinical studies into the clinical setting for the detection and management of cancer in humans.[77] Parahydrogen can be used to hydrogenate multiple bonds in chemical structures containing enriched ^{13}C isotopes (PASADENA) as an alternative mechanism to hyperpolarize ^{13}C nuclei.[79] Hyperpolarization based on parahydrogen requires ^{13}C substrates with a particular chemical structure, limiting its general applicability compared to DNP-based methods.

Recently hyperpolarized ^{13}C-labeled bicarbonate was used to measure tumor pHe in vivo.[80] This approach employs the cellular buffering system to determine pHe. DNP of ^{13}C-bicarbonate increases the sensitivity of ^{13}C detection dramatically, enabling ^{13}C MRSI of tissues in vivo. The ratio of $H^{13}CO_3^-$ to $^{13}CO_2$ provides a measure of tissue pHe, assuming a pKa of 6.17.[80] pHe maps were obtained with a spatial resolution of $2 \times 2 \times 6$ mm^3 in initial preclinical studies.[80] Since the bicarbonate probe is nontoxic, it may, in the future, be translated to the clinic to image pHe for oncological applications.

^1H MRS IN CLINICAL DIAGNOSIS

Most clinical MR scanners have routine sequences for ^1H MRS/I measurements.[11,12,81–83] Quantitative ^1H MRS and ^1H MRSI measurements of tCho and tissue-specific metabolites are frequently implemented in the clinic, in addition to standard dynamic contrast-enhanced (DCE) MR imaging (MRI), to diagnose primary malignant tumors in brain,[7–10] prostate,[11] and breast.[12–14,84] The addition of MRS to standard MRI techniques can significantly increase the sensitivity up to 88%, the specificity to greater than 90%, and the diagnostic accuracy up to 91%. Choline metabolites such as PC, GPC, and Cho, among others, provide robust biomarkers in human biopsy specimens ex vivo using high-resolution ^1H MRS of extracts or HR MAS ^1H MRS of intact specimens. Elevated tCho and PC concentrations have been used to identify meningiomas and recurrent astrocytomas in human brain tissue specimens,[85] breast cancer in fine-needle aspirates of breast tumors,[86] and prostatic carcinoma in postsurgical prostate tissue samples.[6]

The most striking and consistent difference between normal and tumor tissue is in levels of tCho; normal tissues display low tCho levels, whereas tumors display high tCho levels.[12,82,83] Proton MRS and MRSI therefore have been applied clinically to assist in diagnosing cancer, and in specifying the margins of brain,[7,87] prostate,[82,83] and breast[12,20,88] tumors, among others. Additionally, ^1H MRS detection of tCho in the clinical setting can also help distinguish tumor recurrence from necrosis in the brain[89,90] or prostate[91] following anti-cancer therapy. Single-voxel ^1H MRS or multi-voxel ^1H MRSI are

able to detect changes in tCho and other metabolites such as creatine, NAA, and lactate. Therefore, the specificity of detection can be improved by measuring and calculating metabolite ratios. In a recent in vivo study, all metabolite intensities detected in ^{1}H MRSI data were translated into metabolomic profiles by applying prior knowledge from HR MAS ^{1}H MRS data from the same tissue type.[92] Malignancy indices were derived from the in vivo–detected prostate cancer metabolomic profiles, which linearly correlated with lesion size, and achieved up to 97% overall accuracy for detecting prostate cancer lesions.[92]

To identify suspicious lesions in the prostate, several MRI parameters, including T_2-weighted contrast, T_1-weighted DCE-MRI, and diffusion-weighted imaging (DWI) are often combined in current radiological practice. A high T_2-weighted MRI signal is typically detected in normal prostatic tissue, whereas a low T_2-weighted MRI signal has been shown to correlate with pathological prostatic tissue, as demonstrated in Figure 4.[93] In spite of improved visualization of prostate morphology with T_2-weighted MRI at 3T, there remains an urgent need for increased specificity and identification of “functional” cellular and metabolic characteristics of prostate tissue. As shown in Figure 4, this need can be satisfied by incorporating MRSI into the MR exam, where an elevated tCho signal was detected in a newly diagnosed patient with Gleason score 6 prostate cancer, serum prostate-specific antigen level of 4.6 ng/mL, and clinical stage of T2B.[93,94] Inclusion of MRSI can augment the reliable outlining of tumor margins and tumor infiltration into healthy tissue. However, relatively high tCho signals may be detected in a few benign and highly proliferative lesions. Under such circumstances, a differential diagnosis should be based on the clinical data from other diagnostic scans.[12,95] Additionally, single-voxel ^{1}H MRS and multi-voxel ^{1}H MRSI can be applied clinically in treatment planning for radiation[96] or brachytherapy.[97]

^{1}H MRS MONITORING OF CANCER THERAPY: CLINICAL AND PRECLINICAL EXAMPLES

The identification, and effective neutralization, of targets and pathways that present a molecular Achilles heel of cancer cells form the basis of finding effective treatments against cancer. Factors complicating this endeavor arise because each cancer represents an individual disease with a unique molecular makeup and a genomic instability that facilitates adaptation and survival following anticancer treatments. As more critical targets in cancer cells are revealed, a transition is occurring in today’s anticancer therapies from the “sledgehammer” approach of conventional chemo- and radiotherapy toward specific molecular-targeted therapies. The availability of noninvasive imaging techniques is critically important for the success of these molecular-targeted treatments.[98] Imaging is needed to select targeted therapies that would be the most effective against a particular cancer, and to detect the tumor response to a particular therapy.[98] Advances in novel image-guided platforms such as nanoparticles, liposomes, and microencapsulation devices to deliver small interfering RNA (siRNA)[99] or drugs to downregulate cancer-specific targets and pathways are also driven by the initial identification of these cancer-specific targets.

Detecting the early response of a tumor to traditional cytotoxic chemotherapeutic drugs is important to reduce damage to normal tissue in patients with nonresponding tumors, and to alter the therapeutic strategy early on, before completing a full course of treatment. Single-voxel ^{1}H MRS and MRSI have shown utility in assessing treatment response in brain,[10,100] breast,[20] and prostate[82] cancers. Multiple studies have identified changes in tCho as having a high likelihood of detecting early response in breast cancer.[20,101] An example of detecting, and possibly predicting, tumor response based on the tCho signal was demonstrated in patients with locally advanced breast cancer who either responded (Figure 5A), or did not respond (Figure 5B), to neoadjuvant chemotherapy (NACT).[102] An early response of prostate cancer to hormone-deprivation therapy[82,83] and cryosurgery[103] was detected by a

decrease in [tCho/citrate] ratios quantified from ^{1}H MR spectra. Anticancer treatments leading to apoptosis or necrosis induced characteristic changes in choline phospholipid metabolites.[104] An early response to therapy in lymphomas was also associated with a reduction of tCho.[105] Some cancers, eg, cervical cancer, did not exhibit a change in the tCho signal following neoadjuvant therapy and subsequent surgical resection of the tumors.[106] However, these cervical cancers displayed a reduced tumor volume along with decreased triglyceride signal, without any difference in patient survival with or without neoadjuvant therapy, and there was no survival advantage associated with the reduced tumor volume or decreased triglycerides.[106]

Molecular-targeted preclinical studies demonstrate that caution must be exercised when using tCho and PC as surrogate markers to interpret tumor response. While a decrease of tCho and PC was observed following treatments against molecular targets such as mitogen-activated protein kinase (MAPK),[107] fatty acid synthase,[108] and Bcr-Abl tyrosine kinase,[109] PC levels were found to increase following histone deacetylase (HDAC) inhibition.[110] Therefore, a decrease of tCho or PC cannot always be associated with response, as this will depend on the target selected. However, PC levels did not change following HDAC inhibition in tumors in vivo.[110] A novel fluorinated lysine derivative, which is a cleavable substrate for HDAC that can detect HDAC activity monitored by ^{19}F MRS, was also described in the same study.[110]

The high PC levels in tumors are, in large part, caused by an increased expression and activity of Chk. Therefore, Chk presents an attractive molecular target for anticancer therapy.[15,111–113] An advantage of targeting Chk is that its downregulation or inhibition will result directly in a decrease of PC and tCho, which can be detected noninvasively with ^{31}P or ^{1}H MRS.[111,112] Novel pharmacological inhibitors, developed to target Chk,[113] resulted in tumor growth arrest and apoptosis.[18,111] RNA interference (RNAi) also has been used to silence Chk.[15,112]. RNAi is known to facilitate sequence-specific inhibition of gene expression.[114] Small interfering RNA (siRNA), which is small double-stranded RNA of 19 to 23 nucleotides, can target any mRNA to which it is specific, and silence its expression.[114] Silencing Chk-α with siRNA significantly reduced cell proliferation and increased differentiation in highly invasive and metastatic MDA-MB-231 human breast cancer cells but not in nonmalignant immortalized MCF-12A mammary epithelial cells.[15] Gene therapy with an intravenously injected lentiviral vector, which was able to deliver Chk-specific short-hairpin RNA (shRNA) in a breast cancer model, was monitored noninvasively by single-voxel ^{31}P MRS.[112] In this study, a reduction of PC and PME was observed, which indicated that Chk was successfully downregulated by this lentiviral Chk-targeted gene therapy.[112] Chk downregulation was accompanied by a reduction in cell proliferation and tumor growth, demonstrating the feasibility of future gene therapeutic approaches to target Chk in tumors and the ability to detect Chk targeting.[112]

With the implementation of hyperpolarization techniques enabling ^{13}C MRSI, hyperpolarized ^{13}C-labeled substrates, such as [1-^{13}C]-pyruvate and [1,4-$^{13}C_2$]-fumarate, have been investigated for detecting treatment response in a murine lymphoma model.[76,115] Tumor response was detected from the change in the flux of hyperpolarized ^{13}C label between pyruvate and lactate in the case of [1-^{13}C]-pyruvate, and an increase of [1,4-$^{13}C_2$]-malate production in the case of [1,4-$^{13}C_2$]-fumarate.[76,115] The increase of [1,4-$^{13}C_2$]-malate production was attributed to an increase of necrosis. A recent study demonstrated that the tumor response to anticancer drugs that target phosphatidylinositol 3-kinase (PI3K) can be monitored by hyperpolarized [1-^{13}C]-pyruvate-injected, and hyperpolarized [1-^{13}C]-lactate-detected ^{13}C MRS, through alterations in lactate dehydrogenase activity caused by PI3K pathway inhibition.[116]

A major problem in cancer chemotherapy is poor drug delivery. MRS can be used to directly measure pharmacokinetics of drugs that can be given at relatively high concentrations in the tumor.[117,118] Most studies on MR pharmacokinetic measurements of tumors in vivo employ fluorinated drugs such as [5-^{19}F]-fluorouracil (5-FU) detected by ^{19}F MRS,[119] because ^{19}F MRS provides relatively high sensitivity combined with the absence of a background signal. In a recent study, the uptake and metabolism of the chemotherapeutic agent 5-FU was detected in liver metastases from colo-rectal cancer using ^{19}F MRS.[120] Successful image-guided delivery of a prodrug enzyme, bacterial cytosine deaminase (bCD), that converts nontoxic [5-^{19}F]-fluorocytosine (5-FC) to 5-FU was recently reported in preclinical studies.[121] Prodrug enzyme delivery was visualized by conjugating bCD to poly-L-lysine functionalized with biotin, rhodamine, and Gd^{3+}-1,4,7,10-tetraazacyclododecane-1,4,7,10-tetraacetic acid (DOTA) for optical and MR imaging.[121] Damage from the active drug 5-FU was minimized in normal tissue and maximized in the tumor by timing 5-FC prodrug administration under image-guidance to coincide with maximum bCD concentration in the tumor and minimum bCD concentration in normal tissue.[121] ^{19}F MRS was used to detect the conversion of the prodrug 5-FC to the active drug 5-FU.[12]

Drugs that do not contain ^{19}F atoms may be altered in their physicochemical and pharmacological properties by chemical ^{19}F-labeling.[122] Therefore, ^{13}C and ^{1}H MRS methods also are being explored to detect drug uptake and distribution.[123] Such approaches require the ^{13}C-labeled drug to have at least one well-resolved, isolated ^{13}C signal.[124] The ^{13}C-labeled drug has to be administered at relatively high doses to be within the detection sensitivity of MRS.[124] The intratumoral distribution of the ^{13}C-labeled anticancer agent temozolomide was recently imaged by ^{1}H/^{13}C MRS as shown in Figure 6.[123] This ^{13}C MRSI study revealed a heterogeneous delivery of temozolomide to the tumor[123] (Figure 6). In the clinic, temozolomide is used as a chemotherapeutic drug to treat glioblastomas and anaplastic astrocytomas.[125] These preclinical studies using ^{1}H/^{13}C MRSI to detect ^{13}C-labeled temozolomide delivery in a brain tumor model suggest a potential use of future ^{1}H/^{13}C MRS/I techniques in detecting temozolomide delivery in human cancers.[118]

CONCLUSION

The major strengths of MRS are the ability to provide a wide range of metabolic and functional information, and to seamlessly integrate with complementary MRI applications. MRS can fulfill important requirements in cancer discovery and treatment in the current era of personalized and targeted molecular medicine. MRS methods may provide an understanding of the effects of downregulating specific targets on downstream changes in physiology and metabolism, which are a rich source to mine for noninvasive biomarkers associated with molecular targets.

Sensitivity and spectral resolution continue to be limiting factors of today's MRSI techniques. However, the availability of higher field strengths and novel techniques such as hyperpolarization can minimize these limitations. The multiparametric capabilities of MRS methods, and the ease of transitioning from bench to bedside and combining MRS methods with other imaging modalities, make MRS a valuable modality for molecular and functional imaging of cancer. MRS will continue to evolve as a cornerstone technique for personalized medicine in cancer.

Acknowledgments

Supported in part by National Institutes of Health Grants No. R01 CA134695, P50 CA103175, R01 CA73850, R01 CA82337, R01 CA136576, R01 CA138515, R21 CA140904, and R21 CA133600.

References

1. Jemal A, Siegel R, Ward E, Hao Y, Xu J, Thun MJ. Cancer statistics, 2009. CA Cancer J Clin. 2009; 59:225–49. [PubMed: 19474385]
2. Griffin JL, Kauppinen RA. Tumour metabolomics in animal models of human cancer. J Proteome Res. 2007; 6:498–505. [PubMed: 17269706]
3. Glunde K, Serkova NJ. Therapeutic targets and biomarkers identified in cancer choline phospholipid metabolism. Pharmacogenomics. 2006; 7:1109–23. [PubMed: 17054420]
4. Costello LC, Franklin RB. 'Why do tumour cells glycolyse?': from glycolysis through citrate to lipogenesis. Mol Cell Biochem. 2005; 280:1–8. [PubMed: 16511951]
5. Griffin JL, Kauppinen RA. A metabolomics perspective of human brain tumours. FEBS J. 2007; 274:1132–9. [PubMed: 17298437]
6. Swanson MG, Zektzer AS, Tabatabai ZL, et al. Quantitative analysis of prostate metabolites using ^{1}H HR-MAS spectroscopy. Magn Reson Med. 2006; 55:1257–64. [PubMed: 16685733]
7. Ross B, Michaelis T. Clinical applications of magnetic resonance spectroscopy. Magn Reson Q. 1994; 10:191–247. [PubMed: 7873353]
8. Nelson SJ. Analysis of volume MRI and MR spectroscopic imaging data for the evaluation of patients with brain tumors. Magn Reson Med. 2001; 46:228–39. [PubMed: 11477625]
9. Howe FA, Barton SJ, Cudlip SA, et al. Metabolic profiles of human brain tumors using quantitative in vivo ^{1}H magnetic resonance spectroscopy. Magn Reson Med. 2003; 49:223–32. [PubMed: 12541241]
10. Jenkinson MD, Smith TS, Joyce K, et al. MRS of oligodendroglial tumors: correlation with histopathology and genetic subtypes. Neurology. 2005; 64:2085–9. [PubMed: 15985578]
11. Kurhanewicz J, Vigneron DB, Hricak H, Narayan P, Carroll P, Nelson SJ. Three-dimensional H-^{1} MR spectroscopic imaging of the in situ human prostate with high (0.24–0.7-cm^{3}) spatial resolution. Radiology. 1996; 198:795–805. [PubMed: 8628874]
12. Jacobs MA, Barker PB, Bottomley PA, Bhujwalla Z, Bluemke DA. Proton magnetic resonance spectroscopic imaging of human breast cancer: a preliminary study. J Magn Reson Imaging. 2004; 19:68–75. [PubMed: 14696222]
13. Meisamy S, Bolan PJ, Baker EH, et al. Adding in vivo quantitative ^{1}H MR spectroscopy to improve diagnostic accuracy of breast MR imaging: preliminary results of observer performance study at 4.0 T. Radiology. 2005; 236:465–75. [PubMed: 16040903]
14. Stanwell P, Gluch L, Clark D, et al. Specificity of choline metabolites for in vivo diagnosis of breast cancer using ^{1}H MRS at 1.5 T. Eur Radiol. 2005; 15:1037–43. [PubMed: 15351906]
15. Glunde K, Raman V, Mori N, Bhujwalla ZM. RNA interference-mediated choline kinase suppression in breast cancer cells induces differentiation and reduces proliferation. Cancer Res. 2005; 65:11034–43. [PubMed: 16322253]
16. Ramirez de Molina A, Gallego-Ortega D, Sarmentero J, Banez-Coronel M, Martin-Cantalejo Y, Lacal JC. Choline kinase is a novel oncogene that potentiates RhoA-induced carcinogenesis. Cancer Res. 2005; 65:5647–53. [PubMed: 15994937]
17. Ramirez de Molina A, Gutierrez R, Ramos MA, et al. Increased choline kinase activity in human breast carcinomas: clinical evidence for a potential novel antitumor strategy. Oncogene. 2002; 21:4317–22. [PubMed: 12082619]
18. Rodriguez-Gonzalez A, Ramirez de Molina A, Fernandez F, Lacal JC. Choline kinase inhibition induces the increase in ceramides resulting in a highly specific and selective cytotoxic antitumoral strategy as a potential mechanism of action. Oncogene. 2004; 23:8247–59. [PubMed: 15378008]
19. Kurhanewicz J, Vigneron DB, Males RG, Swanson MG, Yu KK, Hricak H. The prostate: MR imaging and spectroscopy. Present and future. Radiol Clin North Am. 2000; 38:115–38. [PubMed: 10664669]
20. Meisamy S, Bolan PJ, Baker EH, et al. Neoadjuvant chemotherapy of locally advanced breast cancer: predicting response with in vivo $^{(1)}$H MR spectroscopy—a pilot study at 4 T. Radiology. 2004; 233:424–31. [PubMed: 15516615]

21. Baek HM, Chen JH, Nie K, et al. Predicting pathologic response to neoadjuvant chemotherapy in breast cancer by using MR imaging and quantitative ^{1}H MR spectroscopy. Radiology. 2009; 251:653–62. [PubMed: 19276320]
22. Glunde K, Jie C, Bhujwalla ZM. Molecular causes of the aberrant choline phospholipid metabolism in breast cancer. Cancer Res. 2004; 64:4270–6. [PubMed: 15205341]
23. Negendank W. Studies of human tumors by MRS: a review. NMR Biomed. 1992; 5:303–24. [PubMed: 1333263]
24. Podo F. Tumour phospholipid metabolism. NMR Biomed. 1999; 12:413–39. [PubMed: 10654290]
25. Ronen SM, Leach MO. Imaging biochemistry: applications to breast cancer. Breast Cancer Res. 2001; 3:36–40. [PubMed: 11250743]
26. Aboagye EO, Bhujwalla ZM. Malignant transformation alters membrane choline phospholipid metabolism of human mammary epithelial cells. Cancer Res. 1999; 59:80–4. [PubMed: 9892190]
27. Iorio E, Mezzanzanica D, Alberti P, et al. Alterations of choline phospholipid metabolism in ovarian tumor progression. Cancer Res. 2005; 65:9369–76. [PubMed: 16230400]
28. Albers MJ, Krieger MD, Gonzalez-Gomez I, et al. Proton-decoupled ^{31}P MRS in untreated pediatric brain tumors. Magn Reson Med. 2005; 53:22–9. [PubMed: 15690498]
29. Arias-Mendoza F, Payne GS, Zakian KL, et al. In vivo ^{31}P MR spectral patterns and reproducibility in cancer patients studied in a multi-institutional trial. NMR Biomed. 2006; 19:504–12. [PubMed: 16763965]
30. Klomp DW, Wijnen JP, Scheenen TW, Heerschap A. Efficient ^{1}H to ^{31}P polarization transfer on a clinical 3T MR system. Magn Reson Med. 2008; 60:1298–305. [PubMed: 19030163]
31. Katz-Brull R, Degani H. Kinetics of choline transport and phosphorylation in human breast cancer cells; NMR application of the zero trans method. Anticancer Res. 1996; 16:1375–80. [PubMed: 8694504]
32. Eliyahu G, Kreizman T, Degani H. Phosphocholine as a biomarker of breast cancer: molecular and biochemical studies. Int J Cancer. 2007; 120:1721–30. [PubMed: 17236204]
33. Noh DY, Ahn SJ, Lee RA, et al. Overexpression of phospholipase D1 in human breast cancer tissues. Cancer Lett. 2000; 161:207–14. [PubMed: 11090971]
34. Foster DA, Xu L. Phospholipase D in cell proliferation and cancer. Mol Cancer Res. 2003; 1:789–800. [PubMed: 14517341]
35. Gillies RJ, Morse DL. In vivo magnetic resonance spectroscopy in cancer. Annu Rev Biomed Eng. 2005; 7:287–326. [PubMed: 16004573]
36. Hakumaki JM, Poptani H, Sandmair AM, Yla-Herttuala S, Kauppinen RA. ^{1}H MRS detects polyunsaturated fatty acid accumulation during gene therapy of glioma: implications for the in vivo detection of apoptosis. Nat Med. 1999; 5:1323–7. [PubMed: 10546002]
37. He Q, Bhujwalla ZM, Glickson JD. Proton detection of choline and lactate in EMT6 tumors by spin-echo-enhanced selective multiple-quantum-coherence transfer. J Magn Reson Series B. 1996; 112:18–25.
38. Melkus G, Morchel P, Behr VC, Kotas M, Flentje M, Jakob PM. Short-echo spectroscopic imaging combined with lactate editing in a single scan. NMR Biomed. 2008; 21:1076–86. [PubMed: 18613250]
39. Thakur SB, Yaligar J, Koutcher JA. In vivo lactate signal enhancement using binomial spectral-selective pulses in selective MQ coherence (SS-SelMQC) spectroscopy. Magn Reson Med. 2009; 62:591–8. [PubMed: 19526486]
40. Engelmann J, Henke J, Willker W, et al. Early stage monitoring of miltefosine induced apoptosis in KB cells by multinuclear NMR spectroscopy. Anticancer Res. 1996; 16:1429–39. [PubMed: 8694511]
41. Al-Saffar NM, Titley JC, Robertson D, et al. Apoptosis is associated with triacylglycerol accumulation in Jurkat T-cells. Br J Cancer. 2002; 86:963–70. [PubMed: 11953830]
42. Barba I, Cabanas ME, Arus C. The relationship between nuclear magnetic resonance-visible lipids, lipid droplets, and cell proliferation in cultured C6 cells. Cancer Res. 1999; 59:1861–8. [PubMed: 10213493]

43. Schmitz JE, Kettunen MI, Hu DE, Brindle KM. ^{1}H MRS-visible lipids accumulate during apoptosis of lymphoma cells in vitro and in vivo. Magn Reson Med. 2005; 54:43–50. [PubMed: 15968678]
44. Vander Heiden MG, Cantley LC, Thompson CB. Understanding the Warburg effect: the metabolic requirements of cell proliferation. Science. 2009; 324:1029–33. [PubMed: 19460998]
45. Okunieff PG, Koutcher JA, Gerweck L, et al. Tumor size dependent changes in a murine fibrosarcoma: use of in vivo ^{31}P NMR for non-invasive evaluation of tumor metabolic status. Int J Radiat Oncol Biol Phys. 1986; 12:793–9. [PubMed: 3710861]
46. Li SJ, Wehrle JP, Rajan SS, Steen RG, Glickson JD, Hilton J. Response of radiation-induced fibrosarcoma-1 in mice to cyclophosphamide monitored by in vivo ^{31}P nuclear magnetic resonance spectroscopy. Cancer Res. 1988; 48:4736–42. [PubMed: 3409214]
47. Kallman RF. The phenomenon of reoxygenation and its implications for fractionated radiotherapy. Radiology. 1972; 105:135–42. [PubMed: 4506641]
48. Tozer GM, Griffiths JR. The contribution made by cell death and oxygenation to ^{31}P MRS observations of tumour energy metabolism. NMR Biomed. 1992; 5:279 – 89. [PubMed: 1449969]
49. Moon RB, Richards JH. Determination of intracellular pH by ^{31}P magnetic resonance. J Biol Chem. 1973; 248:7276–8. [PubMed: 4743524]
50. Stubbs M, Bhujwalla ZM, Tozer GM, et al. An assessment of ^{31}P MRS as a method of measuring pH in rat tumours. NMR Biomed. 1992; 5:351–9. [PubMed: 1489671]
51. Vaupel P, Kallinowski F, Okunieff P. Blood flow, oxygen and nutrient supply, and metabolic microenvironment of human tumors: a review. Cancer Res. 1989; 49:6449–65. [PubMed: 2684393]
52. Griffiths JR. Are cancer cells acidic? Br J Cancer. 1991; 64:425–7. [PubMed: 1911181]
53. Gillies RJ, Liu Z, Bhujwalla ZM. ^{31}P-MRS measurements of extracellular pH of tumors using 3-aminopropylphosphonate. Am J Physiol. 1994; 267:C195–203. [PubMed: 8048479]
54. van Sluis R, Bhujwalla ZM, Raghunand N, et al. In vivo imaging of extracellular pH using ^{1}H MRSI. Magn Reson Med. 1999; 41:743–50. [PubMed: 10332850]
55. Martinez-Zaguilan R, Seftor EA, Seftor RE, Chu YW, Gillies RJ, Hendrix MJ. Acidic pH enhances the invasive behavior of human melanoma cells. Clin Exp Metastasis. 1996; 14:176–86. [PubMed: 8605731]
56. Raghunand N, Mahoney B, van Sluis R, Baggett B, Gillies RJ. Acute metabolic alkalosis enhances response of C3H mouse mammary tumors to the weak base mitoxantrone. Neoplasia. 2001; 3:227–35. [PubMed: 11494116]
57. Robey IF, Baggett BK, Kirkpatrick ND, et al. Bicarbonate increases tumor pH and inhibits spontaneous metastases. Cancer Res. 2009; 69:2260–8. [PubMed: 19276390]
58. Gil S, Zaderenzo P, Cruz F, Cerdan S, Ballesteros P. Imidazol-1-ylalkanoic acids as extrinsic ^{1}H NMR probes for the determination of intracellular pH, extracellular pH and cell volume. Bioorg Med Chem. 1994; 2:305–14. [PubMed: 7922141]
59. Bhujwalla ZM, Artemov D, Ballesteros P, Cerdan S, Gillies RJ, Solaiyappan M. Combined vascular and extracellular pH imaging of solid tumors. NMR Biomed. 2002; 15:114–9. [PubMed: 11870907]
60. Ojugo AS, McSheehy PM, McIntyre DJ, et al. Measurement of the extracellular pH of solid tumours in mice by magnetic resonance spectroscopy: a comparison of exogenous $^{(19)}$F and $^{(31)}$P probes. NMR Biomed. 1999; 12:495–504. [PubMed: 10668042]
61. Provent P, Benito M, Hiba B, et al. Serial in vivo spectroscopic nuclear magnetic resonance imaging of lactate and extracellular pH in rat gliomas shows redistribution of protons away from sites of glycolysis. Cancer Res. 2007; 67:7638–45. [PubMed: 17699768]
62. Cheng LL, Burns MA, Taylor JL, et al. Metabolic characterization of human prostate cancer with tissue magnetic resonance spectroscopy. Cancer Res. 2005; 65:3030–4. [PubMed: 15833828]
63. Sitter B, Lundgren S, Bathen TF, Halgunset J, Fjosne HE, Gribbestad IS. Comparison of HR MAS MR spectroscopic profiles of breast cancer tissue with clinical parameters. NMR Biomed. 2006; 19:30–40. [PubMed: 16229059]

64. Martinez-Bisbal MC, Marti-Bonmati L, Piquer J, et al. ^{1}H and ^{13}C HR-MAS spectroscopy of intact biopsy samples ex vivo and in vivo ^{1}H MRS study of human high grade gliomas. NMR Biomed. 2004; 17:191–205. [PubMed: 15229932]
65. Bathen TF, Jensen LR, Sitter B, et al. MR-determined metabolic phenotype of breast cancer in prediction of lymphatic spread, grade, and hormone status. Breast Cancer Res Treat. 2007; 104:181–9. [PubMed: 17061040]
66. Artemov D, Bhujwalla ZM, Glickson JD. In vivo selective measurement of (1-^{13}C)-glucose metabolism in tumors by heteronuclear cross polarization. Magn Reson Med. 1995; 33:151–5. [PubMed: 7707903]
67. van Zijl PC, Chesnick AS, DesPres D, Moonen CT, Ruiz-Cabello J, van Gelderen P. In vivo proton spectroscopy and spectroscopic imaging of [1-^{13}C]-glucose and its metabolic products. Magn Reson Med. 1993; 30:544–51. [PubMed: 8259054]
68. Kim JW, Dang CV. Cancer's molecular sweet tooth and the Warburg effect. Cancer Res. 2006; 66:8927–30. [PubMed: 16982728]
69. Semenza GL. Oxygen-dependent regulation of mitochondrial respiration by hypoxia-inducible factor 1. Biochem J. 2007; 405:1–9. [PubMed: 17555402]
70. Vaupel P, Okunieff P, Kallinowski F, Neuringer LJ. Correlations between ^{31} P-NMR spectroscopy and tissue O_2 tension measurements in a murine fibrosarcoma. Radiat Res. 1989; 120:477–93. [PubMed: 2594969]
71. Macheda ML, Rogers S, Best JD. Molecular and cellular regulation of glucose transporter (GLUT) proteins in cancer. J Cell Physiol. 2005; 202:654–62. [PubMed: 15389572]
72. Rivenzon-Segal D, Margalit R, Degani H. Glycolysis as a metabolic marker in orthotopic breast cancer, monitored by in vivo (13)C MRS. Am J Physiol Endocrinol Metab. 2002; 283:E623–30. [PubMed: 12217878]
73. Terpstra M, High WB, Luo Y, de Graaf RA, Merkle H, Garwood M. Relationships among lactate concentration, blood flow and histopathologic profiles in rat C6 glioma. NMR Biomed. 1996; 9:185–94. [PubMed: 9067999]
74. Nielsen FU, Daugaard P, Bentzen L, et al. Effect of changing tumor oxygenation on glycolytic metabolism in a murine C^{3}H mammary carcinoma assessed by in vivo nuclear magnetic resonance spectroscopy. Cancer Res. 2001; 61:5318–25. [PubMed: 11431377]
75. Bouzier AK, Quesson B, Valeins H, Canioni P, Merle M. [1-(13)C]glucose metabolism in the tumoral and nontumoral cerebral tissue of a glioma-bearing rat. J Neurochem. 1999; 72:2445–55. [PubMed: 10349854]
76. Day SE, Kettunen MI, Gallagher FA, et al. Detecting tumor response to treatment using hyperpolarized ^{13}C magnetic resonance imaging and spectroscopy. Nat Med. 2007; 13:1382–7. [PubMed: 17965722]
77. Albers MJ, Bok R, Chen AP, et al. Hyperpolarized ^{13}C lactate, pyruvate, and alanine: noninvasive biomarkers for prostate cancer detection and grading. Cancer Res. 2008; 68:8607–15. [PubMed: 18922937]
78. Ardenkjaer-Larsen JH, Fridlund B, Gram A, et al. Increase in signal-to-noise ratio of > 10,000 times in liquid-state NMR. Proc Natl Acad Sci U S A. 2003; 100:10158–63. [PubMed: 12930897]
79. Goldman M, Johannesson H, Axelsson O, Karlsson M. Hyperpolarization of ^{13}C through order transfer from parahydrogen: a new contrast agent for MRI. Magn Reson Imaging. 2005; 23:153–7. [PubMed: 15833606]
80. Gallagher FA, Kettunen MI, Day SE, et al. Magnetic resonance imaging of pH in vivo using hyperpolarized ^{13}C-labelled bicarbonate. Nature. 2008; 453:940–3. [PubMed: 18509335]
81. Gill SS, Thomas DG, Van Bruggen N, et al. Proton MR spectroscopy of intracranial tumours: in vivo and in vitro studies. J Comput Assist Tomogr. 1990; 14:497–504. [PubMed: 2164536]
82. Kurhanewicz J, Vigneron DB, Nelson SJ. Three-dimensional magnetic resonance spectroscopic imaging of brain and prostate cancer. Neoplasia. 2000; 2:166–89. [PubMed: 10933075]
83. Mueller-Lisse UG, Swanson MG, Vigneron DB, et al. Time-dependent effects of hormone-deprivation therapy on prostate metabolism as detected by combined magnetic resonance imaging and 3D magnetic resonance spectroscopic imaging. Magn Reson Med. 2001; 46:49–57. [PubMed: 11443710]

84. Jacobs MA, Barker PB, Argani P, Ouwerkerk R, Bhujwalla ZM, Bluemke DB. Combined dynamic contrast and spectroscopic imaging of human breast cancer. J Magn Reson Imaging. 2005; 21:23–8. [PubMed: 15611934]
85. Lehnhardt FG, Bock C, Rohn G, Ernestus RI, Hoehn M. Metabolic differences between primary and recurrent human brain tumors: a ^{1}H NMR spectroscopic investigation. NMR Biomed. 2005; 18:371–82. [PubMed: 15959923]
86. Mountford CE, Somorjai RL, Malycha P, et al. Diagnosis and prognosis of breast cancer by magnetic resonance spectroscopy of fine-needle aspirates analysed using a statistical classification strategy. Br J Surg. 2001; 88:1234–40. [PubMed: 11531873]
87. Li X, Lu Y, Pirzkall A, McKnight T, Nelson SJ. Analysis of the spatial characteristics of metabolic abnormalities in newly diagnosed glioma patients. J Magn Reson Imaging. 2002; 16:229–37. [PubMed: 12205577]
88. Hu J, Vartanian SA, Xuan Y, Latif Z, Soulen RL. An improved ^{1}H magnetic resonance spectroscopic imaging technique for the human breast: preliminary results. Magn Reson Imaging. 2005; 23:571–6. [PubMed: 15919603]
89. Wald LL, Nelson SJ, Day MR, et al. Serial proton magnetic resonance spectroscopy imaging of glioblastoma multiforme after brachytherapy. J Neurosurg. 1997; 87:525–34. [PubMed: 9322843]
90. Laprie A, Pirzkall A, Haas-Kogan DA, et al. Longitudinal multivoxel MR spectroscopy study of pediatric diffuse brainstem gliomas treated with radiotherapy. Int J Radiat Oncol Biol Phys. 2005; 62:20–31. [PubMed: 15850898]
91. Kurhanewicz J, Swanson MG, Nelson SJ, Vigneron DB. Combined magnetic resonance imaging and spectroscopic imaging approach to molecular imaging of prostate cancer. J Magn Reson Imaging. 2002; 16:451–63. [PubMed: 12353259]
92. Wu C-L, Jordan KW, Ratai EM, et al. Metabolomic imaging for human prostate cancer detection. Sci Transl Med. 2010; 2:1–7.
93. Joseph T, McKenna DA, Westphalen AC, et al. Pretreatment endorectal magnetic resonance imaging and magnetic resonance spectroscopic imaging features of prostate cancer as predictors of response to external beam radiotherapy. Int J Radiat Oncol Biol Phys. 2009; 73:665–71. [PubMed: 18760545]
94. Jacobs MA, Ouwerkerk R, Petrowski K, Macura KJ. Diffusion-weighted imaging with apparent diffusion co-efficient mapping and spectroscopy in prostate cancer. Top Magn Reson Imagin. 2008; 19:261–72.
95. Loening NM, Chamberlin AM, Zepeda AG, Gonzalez RG, Cheng LL. Quantification of phosphocholine and glycerophosphocholine with ^{31}P edited ^{1}H NMR spectroscopy. NMR Biomed. 2005; 18:413–20. [PubMed: 16075415]
96. Nelson SJ, Graves E, Pirzkall A, et al. In vivo molecular imaging for planning radiation therapy of gliomas: an application of ^{1}H MRSI. J Magn Reson Imaging. 2002; 16:464–76. [PubMed: 12353260]
97. Zaider M, Zelefsky MJ, Lee EK, et al. Treatment planning for prostate implants using magnetic-resonance spectroscopy imaging. Int J Radiat Oncol Biol Phys. 2000; 47:1085–96. [PubMed: 10863082]
98. Weissleder R, Pittet MJ. Imaging in the era of molecular oncology. Nature. 2008; 452:580–9. [PubMed: 18385732]
99. Medarova Z, Pham W, Farrar C, Petkova V, Moore A. In vivo imaging of siRNA delivery and silencing in tumors. Nat Med. 2007; 13:372–7. [PubMed: 17322898]
100. Law M, Cha S, Knopp EA, Johnson G, Arnett J, Litt AW. High-grade gliomas and solitary metastases: differentiation by using perfusion and proton spectroscopic MR imaging. Radiology. 2002; 222:715–21. [PubMed: 11867790]
101. Haddadin IS, McIntosh A, Meisamy S, et al. Metabolite quantification and high-field MRS in breast cancer. NMR Biomed. 2009; 22:65–76. [PubMed: 17957820]
102. Danishad KK, Sharma U, Sah RG, Seenu V, Parshad R, Jagannathan NR. Assessment of therapeutic response of locally advanced breast cancer (LABC) patients undergoing neoadjuvant chemotherapy (NACT) monitored using sequential magnetic resonance spectroscopic imaging (MRSI). NMR Biomed. 2010; 23:233–241. [PubMed: 20175134]

103. Kurhanewicz J, Vigneron DB, Hricak H, et al. Prostate cancer: metabolic response to cryosurgery as detected with 3D H-1 MR spectroscopic imaging. Radiology. 1996; 200:489–96. [PubMed: 8685346]
104. Evelhoch JL, Gillies RJ, Karczmar GS, et al. Applications of magnetic resonance in model systems: cancer therapeutics. Neoplasia. 2000; 2:152–65. [PubMed: 10933074]
105. Schwarz AJ, Maisey NR, Collins DJ, Cunningham D, Huddart R, Leach MO. Early in vivo detection of metabolic response: a pilot study of ^{1}H MR spectroscopy in extracranial lymphoma and germ cell tumours. Br J Radiol. 2002; 75:959–66. [PubMed: 12515704]
106. deSouza NM, Soutter WP, Rustin G, et al. Use of neo-adjuvant chemotherapy prior to radical hysterectomy in cervical cancer: monitoring tumour shrinkage and molecular profile on magnetic resonance and assessment of 3-year outcome. Br J Cancer. 2004; 90:2326–31. [PubMed: 15162152]
107. Beloueche-Babari M, Jackson LE, Al-Saffar NM, Workman P, Leach MO, Ronen SM. Magnetic resonance spectroscopy monitoring of mitogen-activated protein kinase signaling inhibition. Cancer Res. 2005; 65:3356–63. [PubMed: 15833869]
108. Ross J, Najjar AM, Sankaranarayanapillai M, Tong WP, Kaluarachchi K, Ronen SM. Fatty acid synthase inhibition results in a magnetic resonance-detectable drop in phosphocholine. Mol Cancer Ther. 2008; 7:2556–65. [PubMed: 18723500]
109. Klawitter J, Anderson N, Klawitter J, et al. Time-dependent effects of imatinib in human leukaemia cells: a kinetic NMR-profiling study. Br J Cancer. 2009; 100:923–31. [PubMed: 19259085]
110. Sankaranarayanapillai M, Tong WP, Yuan Q, et al. Monitoring histone deacetylase inhibition in vivo: noninvasive magnetic resonance spectroscopy method. Mol Imaging. 2008; 7:92–100. [PubMed: 18706291]
111. Al-Saffar NM, Troy H, Ramirez de Molina A, et al. Non-invasive magnetic resonance spectroscopic pharmacodynamic markers of the choline kinase inhibitor MN58b in human carcinoma models. Cancer Res. 2006; 66:427–34. [PubMed: 16397258]
112. Krishnamachary B, Glunde K, Wildes F, et al. Noninvasive detection of lentiviral-mediated choline kinase targeting in a human breast cancer xenograft. Cancer Res. 2009; 69:3464–71. [PubMed: 19336572]
113. Lacal JC. Choline kinase: a novel target for antitumor drugs. IDrugs. 2001; 4:419–26. [PubMed: 16015482]
114. Meister G, Tuschl T. Mechanisms of gene silencing by double-stranded RNA. Nature. 2004; 431:343–9. [PubMed: 15372041]
115. Gallagher FA, Kettunen MI, Hu DE, et al. Production of hyperpolarized [1,4-$^{13}C_2$]malate from [1,4-$^{13}C_2$]fumarate is a marker of cell necrosis and treatment response in tumors. Proc Natl Acad Sci U S A. 2009; 106:19801–6. [PubMed: 19903889]
116. Ward CS, Venkatesh HS, Chaumeil MM, et al. Noninvasive detection of target modulation following phosphatidylinositol 3-kinase inhibition using hyperpolarized ^{13}C magnetic resonance spectroscopy. Cancer Res. 2010; 70:1296–305. [PubMed: 20145128]
117. Artemov D, Solaiyappan M, Bhujwalla ZM. Magnetic resonance pharmacoangiography to detect and predict chemotherapy delivery to solid tumors. Cancer Res. 2001; 61:3039–44. [PubMed: 11306485]
118. Kato Y, Holm DA, Okollie B, Artemov D. Noninvasive detection of temozolomide in brain tumor xenografts by magnetic resonance spectroscopy. Neuro Oncol. 2010; 12:71–9. [PubMed: 20150369]
119. Wolf W, Presant CA, Waluch V. ^{19}F-MRS studies of fluorinated drugs in humans. Adv Drug Deliv Rev. 2000; 41:55–74. [PubMed: 10699305]
120. van Laarhoven HW, Klomp DW, Rijpkema M, et al. Prediction of chemotherapeutic response of colorectal liver metastases with dynamic gadolinium-DTPA-enhanced MRI and localized ^{19}F MRS pharmacokinetic studies of 5-fluorouracil. NMR Biomed. 2007; 20:128–40. [PubMed: 17006886]
121. Li C, Penet MF, Winnard P Jr, Artemov D, Bhujwalla ZM. Image-guided enzyme/prodrug cancer therapy. Clin Cancer Res. 2008; 14:515–22. [PubMed: 18223227]

122. Reid DG, Murphy PS. Fluorine magnetic resonance in vivo: a powerful tool in the study of drug distribution and metabolism. Drug Discov Today. 2008; 13:473–80. [PubMed: 18549972]

123. Kato Y, Okollie B, Artemov D. Noninvasive $^{1}H/^{13}C$ magnetic resonance spectroscopic imaging of the intratumoral distribution of temozolomide. Magn Reson Med. 2006; 55:755–61. [PubMed: 16508914]

124. Griffiths JR, Glickson JD. Monitoring pharmacokinetics of anticancer drugs: non-invasive investigation using magnetic resonance spectroscopy. Adv Drug Deliv Rev. 2000; 41:75–89. [PubMed: 10699306]

125. O'Reilly SM, Newlands ES, Glaser MG, et al. Temozolomide: a new oral cytotoxic chemotherapeutic agent with promising activity against primary brain tumours. Eur J Cancer. 1993; 29A:940–2. [PubMed: 8499146]

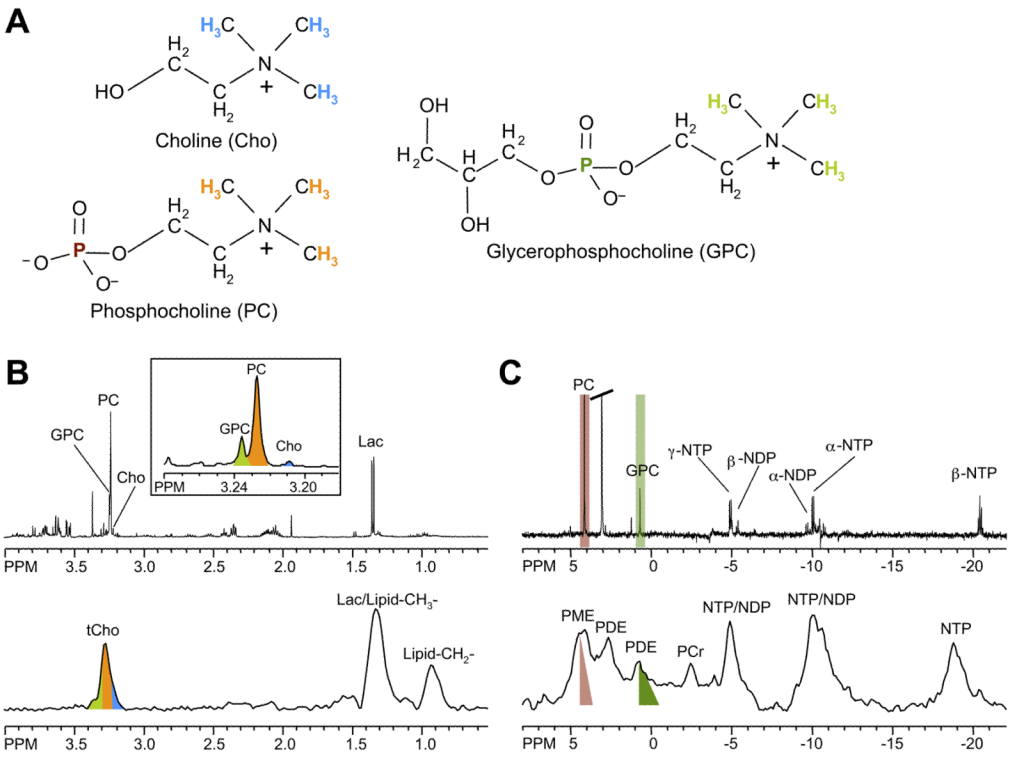

Figure 1.

(A) Chemical structures of the choline phospholipid metabolites free choline (Cho), phosphocholine (PC), and glycerophosphocholine (GPC). (B) High-resolution ex vivo ^{1}H MR spectra of triple-negative human MDA-MB-231 breast cancer cell extracts (top) and in vivo ^{1}H MR spectra of the same cell line grown as orthotopic tumor (bottom). (C) High-resolution ex vivo ^{31}P MR spectra of triple-negative human MDA-MB-231 breast cancer cell extracts (top) and in vivo ^{31}P MR spectra of the same cell line grown as orthotopic tumor (bottom). Cho, free choline; GPC, glycerophosphocholine; GPE, glycerophosphoethanolamine; DPDE, diphosphodiester; NDP, nucleoside diphosphate; NTP, nucleoside triphosphate; Lac, lactate; Lipid-CH_2-, methylene groups of mobile lipids; Lipid-CH_3-, methyl groups of mobile lipids; PC, phosphocholine; PE, phosphoethanolamine; PCr, phosphocreatine; Pi, inorganic phosphate; tCho, total choline-containing compounds (Cho+PC+GPC). The ^{1}H and ^{31}P nuclei in Cho, PC, and GPC and their respective ^{1}H and ^{31}P signals in the MR spectra are color-coded to identify the MR signals that arise from the corresponding nuclei.

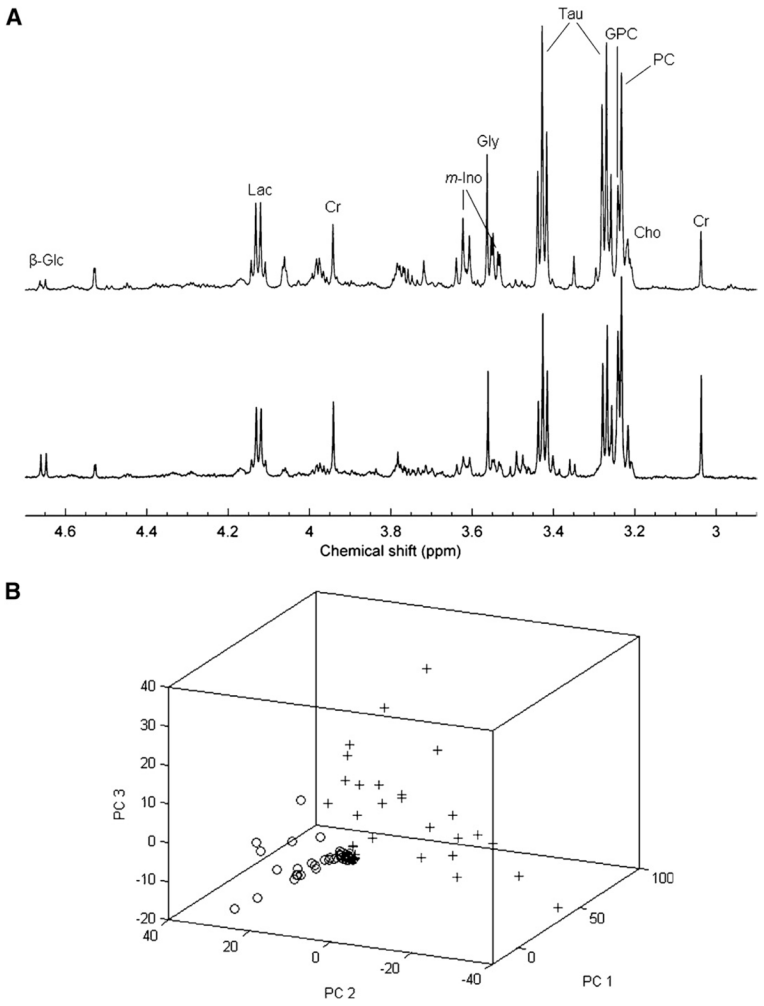

Figure 2.

(A) Region of representative HR MAS $>^{1}$H MRS spectra selected for multivariate analysis, obtained from primary tumor tissue from patients with invasive ductal carcinoma grade III breast cancer. The top spectrum is derived from a patient diagnosed as hormone positive, with lymphatic spread, and the bottom spectrum from a hormone positive patient, without proven lymphatic spread. Glc, glucose; Lac, lactate; Cr, creatine; m-Ino, *myo*-inositol; Tau, taurine; GPC, glycerophosphocholine; PC, phosphocholine; Cho, choline. (B) Score plot of principal component 1 (PC1), principal component 2 (PC2), and principal component (PC3) from the principal component analysis of samples from 77 breast cancer patients. Samples from noninvolved adjacent tissue (0) are separated from the rest, thus demonstrating a marked metabolic difference from the malignant samples (+). However, invasive ductal carcinoma samples were interspersed, and there was no possibility to differentiate them from noninvolved adjacent tissue or cancer, emphasizing the need for more sophisticated analysis in order to achieve classification. Adapted with kind permission from Springer Science +Business Media: Bathen et al.[65]

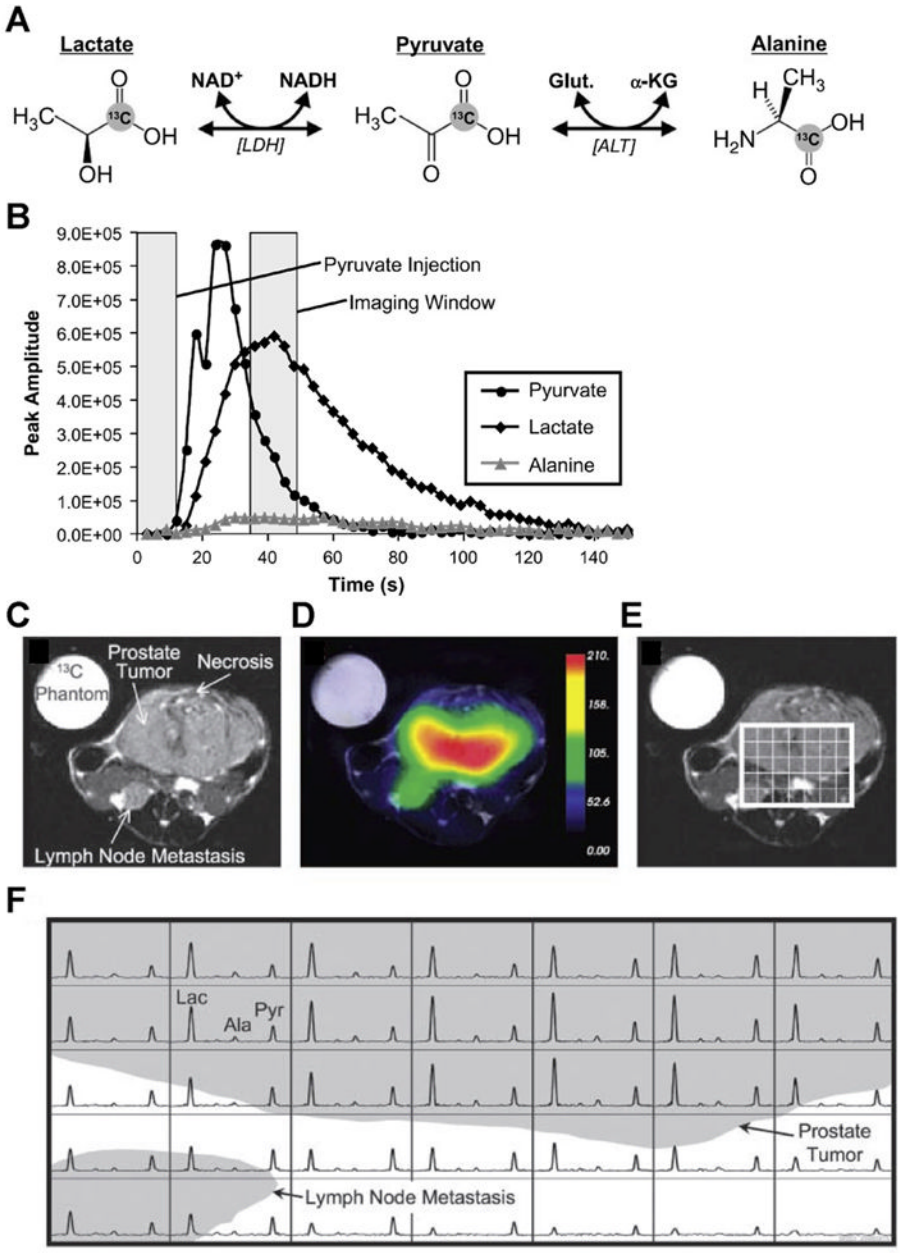

Figure 3.

(A) Diagram of [1-^{13}C]-pyruvate and its relevant metabolic pathways leading to [1-^{13}C]-lactate and [1-^{13}C]-alanine. (B) Peak height plots from hyperpolarized ^{13}C spectra reveal the time course of hyperpolarized [1-^{13}C]-pyruvate and its metabolic products following injection of 28 μmol of hyperpolarized [1-^{13}C]-pyruvate at a constant rate from 0 to 12 s. (C) Axial T_2-weighted 1H MR image showing the primary tumor and a lymph node metastasis in a 'transgenic adenocarcinoma of mouse prostate' (TRAMP) mouse with a high-grade primary tumor, and (D) overlay of an interpolated hyperpolarized [1-^{13}C]-lactate image following injection of 28 μmol of hyperpolarized [1-^{13}C]-pyruvate. After spatially zero-filling and voxel-shifting the ^{13}C MR spectra to maximize the amount of tumor in the voxels, (E) a subset of the spectral grid was selected and (F) displayed. The three-dimensional MRSI was acquired with a nominal voxel size of 135 mm^3, zero-filled to 17

mm^3. Substantially elevated lactate was detected in the high-grade primary tumor compared with adjacent normal tissue. In addition, the metabolite signal is significantly lower in the necrotic regions of the primary tumor. Lac, lactate; Ala, alanine; Pyr, pyruvate. Adapted with permission from the American Association for Cancer Research.[77]

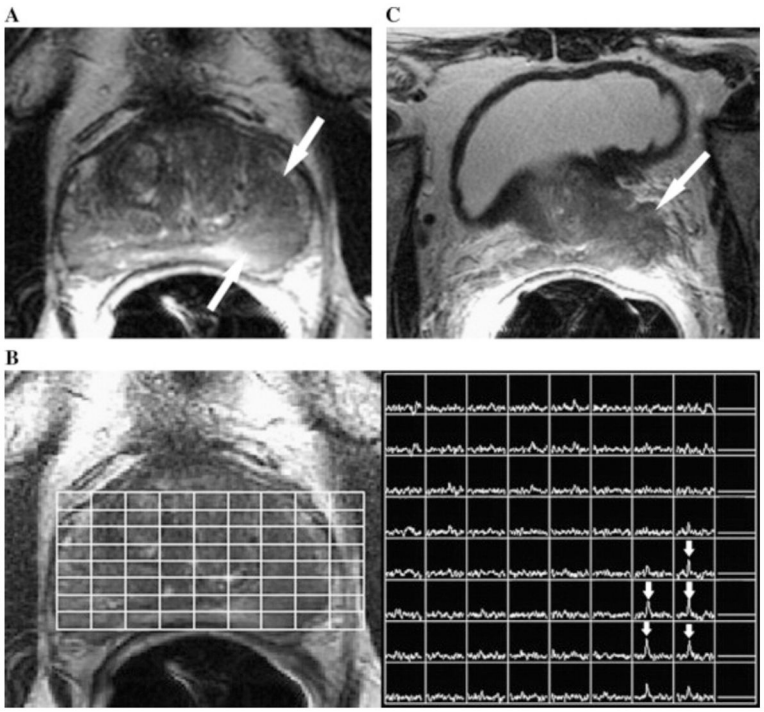

Figure 4.

(A) Axial T_2-weighted 1H MRI section in a 68-year-old man with newly diagnosed Gleason 6 prostate cancer, serum prostate-specific antigen level of 4.6 ng/mL, and clinical stage of T2B. A large focus (arrows) of reduced T_2 signal intensity was observed in the left peripheral zone of the prostate. (B) Photomontage showing the axial T_2-weighted 1H MR image on the left side with an overlaid grid that corresponds to the MRSI spectral array on the right side. Voxels corresponding to the focus of reduced T_2 signal intensity displayed high total choline peaks (arrows), consistent with prostate cancer. (C) Axial T_2-weighted ^{1}H MRI section through the base of the prostate shows gross extracapsular extension of the tumor, with seminal vesicle invasion (stage T3B). The patient developed metastatic recurrence at 21 months after external beam radiotherapy. Adapted from Joseph et al[93] with permission from Elsevier.

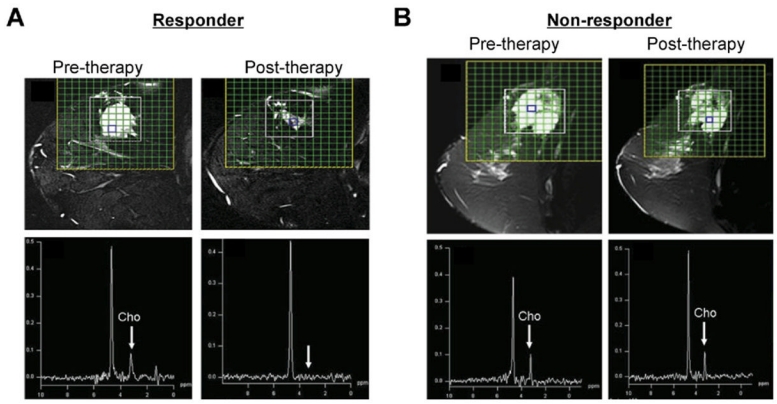

Figure 5.

(A) A pre-therapy T_2-weighted sagittal fat suppressed 1H MR image including MRSI grid is shown that was measured in a patient with locally advanced breast cancer who responded to neoadjuvant chemotherapy (NACT). The ^{1}H MR spectrum on the left was obtained from a voxel with tCho signal prior to therapy. On the right, a post-therapy ^{1}H MR spectrum obtained from the voxel highlighted in the ^{1}H MR image is displayed that was obtained from the same patient after the third cycle of NACT and showed no tCho. (B) Pre-therapy T_2-weighted sagittal fat suppressed 1H MR image with MRSI grid of a patient with locally advanced breast cancer who did not respond to NACT. The ^{1}H MR spectrum on the left was obtained from a voxel highlighted in the above image showing tCho signal. On the right, a post-therapy T_2-weighted sagittal fat suppressed 1H MR image, including a ^{1}H MR spectrum obtained from the highlighted voxel, is displayed that was measured in the same patient after the third cycle of NACT showing tCho signal. These presented data suggest that the tCho signal can predict the response of breast cancer patients to NACT. Adapted with permission from John Wiley and Sons.[102]

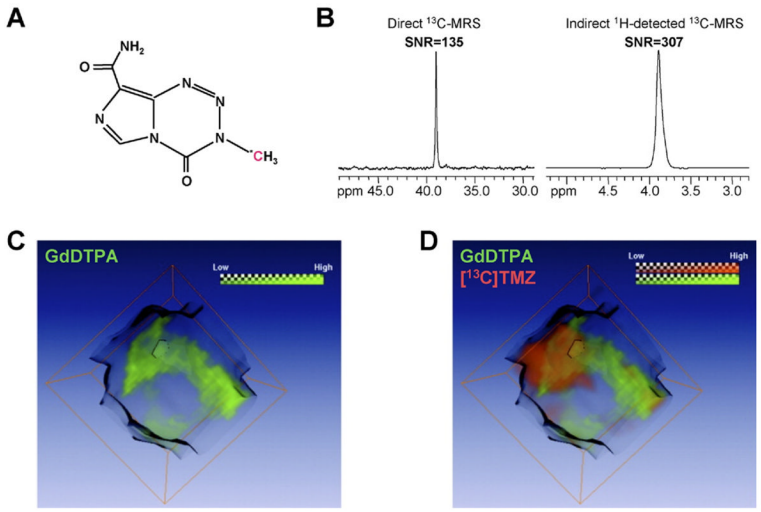

Figure 6.

^{1}H/^{13}C MRSI of ^{13}C-labeled temozolomide ([^{13}C]TMZ) in a human MCF-7 breast tumor xenograft, using the indirect detection technique, heteronuclear multiple-quantum coherence (HMQC). The same tumor was imaged using gadolinium(III) diethylene triamine penta-acetic acid (GdDTPA)-enhanced DCE-MRI. (A) The chemical structure of [^{13}C]TMZ shows the ^{13}C-labeled nucleus. (B) A significantly higher signal-to-noise (SNR) ratio was detected by indirect ^{1}H-detected ^{13}C MRS detection of [^{13}C]TMZ using HMQC as compared to direct ^{13}C MRS detected [^{13}C]TMZ. (C) The corresponding GdDTPA contrast uptake map shown in green was reconstructed as a difference map between pre- and post-contrast acquisitions. The grayscale image represents the tumor. (D) The intratumoral 3D distribution of GdDTPA-contrast uptake (green) was co-registered with the HMQC CSI detected 3D distribution of [^{13}C]TMZ shown in red. Green and red channels indicate the GdDTPA uptake and distribution of [^{13}C]TMZ, respectively, and reveal a partial overlap of the GdDTPA-enhancing regions with tumor areas of high temozolomide uptake. Adapted with permission from John Wiley and Sons.[123]

Table 1

Commonly Studied MR-Detectable Nuclei

Nucleus	γ [MHz/T]	Detected Metabolite or Property	Preclinically Available	Clinically Available
^{1}H	42.58	Total choline	Yes	Yes
		Lactate	Yes	No
		Lipid	Yes	Yes
		N-acetyl-aspartate	Yes	Yes
		Citrate	Yes	Yes
		Extracellular pH (pHe)	Yes	No
		Treatment efficacy	Yes	No
		Detection of metastasis	Yes	No
		Tissue oxygen (pO_2)	Yes	No
^{19}F	40.08	Drug pharmacokinetics	Yes	Yes
		pHe	Yes	No
		pO_2	Yes	No
		Enzyme activity	Yes	No
		Labeled substrate utilization	Yes	No
^{31}P	17.25	Energy metabolism (NTP, PCr, Pi)	Yes	Yes
		Intracellular pH (pHi)	Yes	Yes
		Phospholipid metabolism	Yes	Yes
^{13}C	10.71	Labeled substrate (drug pharmaco kinetics, metabolic pathways)	Yes	Yes

MR-detectable nuclei that are commonly studied are displayed in the order of their detection sensitivity, together with some of their preclinical and clinical applications in cancer. The detection limits of ^{1}H and ^{19}F MRS are typically within the millimolar range of the detected metabolite, with higher concentrations required for less sensitive nuclei such as ^{31}P and ^{13}C.

Abbreviations: NTPs, nucleoside diphosphates; PCr, phosphocreatine; Pi, inorganic phosphate.